

# **B.TECH PROJECT REPORT**

**On**

## **A Theoretical and Computational Study of $\text{CaFe}_x\text{Mn}_{1-x}\text{O}_3$ Perovskites and their Applications**

**BY**  
**Sai Murali Karthik Putcha**



**DEPARTMENT OF METALLURGY ENGINEERING AND  
MATERIALS SCIENCE**  
**INDIAN INSTITUTE OF TECHNOLOGY INDORE**  
**May, 2021**



# **A Theoretical and Computational Study of $\text{CaFe}_x\text{Mn}_{1-x}\text{O}_3$ Perovskites and their Applications**

## **A PROJECT REPORT**

*Submitted in partial fulfillment of the requirements for the award of the  
degree*

*of*

**BACHELOR OF TECHNOLOGY**

**in**

**METALLURGY ENGINEERING AND MATERIALS SCIENCE**

*Submitted by:*

**Sai Murali Karthik Putcha**

*Guided by:*

**Dr. Mrigendra Dubey**

Assistant Professor, Dept. of MEMS, IIT Indore

**Dr. Srimanta Pakhira**

Assistant Professor, Discipline of Physics, IIT Indore

Ramanujan Faculty, Dept. of MEMS, IIT Indore.



**INDIAN INSTITUTE OF TECHNOLOGY INDORE**

May, 2021



## **CANDIDATE'S DECLARATION**

I hereby declare that the project entitled "**A Theoretical and Computational Study of CaFe<sub>x</sub>Mn<sub>1-x</sub>O<sub>3</sub> Perovskites and their Applications**" submitted in partial fulfillment for the award of the degree of Bachelor of Technology in '**Metallurgy Engineering and Materials Science**' completed under the supervision of **Dr. Srimanta Pakhira, Assistant Professor, Discipline of Physics, IIT Indore; Ramanujan Faculty, Department of MEMS, IIT Indore, and Dr. Mrigendra Dubey, Assistant Professor, Department of MEMS, IIT Indore**, is an authentic work.

Further, I declare that I have not submitted this work for the award of any other degree elsewhere.



23/05/2021

**P. SAI MURALI KARTHIK**

**Signature and name of the student with date**

---

## **CERTIFICATE by BTP Guides**

It is certified that the above statement made by the students is correct to the best of our knowledge.

**Signature of BTP Guides with dates and their designation**



## **Preface**

This report on “**A Theoretical and Computational Study of  $\text{CaFe}_x\text{Mn}_{1-x}\text{O}_3$  Perovskites and their Applications**” is prepared under the guidance of **Dr. Srimanta Pakhira, Assistant Professor, Discipline of Physics, IIT Indore; Ramanujan Faculty, Department of MEMS, IIT Indore, and Dr. Mrigendra Dubey, Assistant Professor, Department of MEMS, IIT Indore.**

Through this report we have tried to figure out if doping iron in  $\text{CaMnO}_3$  would enable it to act as bifunctional electrocatalyst for both ORR and OER.

I have tried to the best of our abilities and knowledge to explain the content in a lucid manner. I have also added diagrams, charts and tables to make it more illustrative.

**Sai Murali Karthik Putcha,**  
B.Tech. IV Year,  
Department of Metallurgy Engineering and Materials Science,  
IIT Indore.



## Acknowledgements

I wish to thank Dr. Mrigendra Dubey and Dr. Srimanta Pakhira for their kind support and valuable guidance. It is their help, patience, and support, due to which I was able to complete the theoretical calculations and technical report.

I would like to thank the members of the "Theoretical Condensed Matter Physics And Advanced Computational Materials Science Laboratory", that I was a part of while doing this work, for their help with getting me acquainted with the procedure of performing the calculations that were crucial for this study.

I also wish to thank IIT Indore for providing the facilities such as the MEMS Cluster, and the library which provided access to many journals and other tools.

Without all this support all the work presented in this report would not have been possible.

**Sai Murali Karthik Putcha,**  
B.Tech. IV Year,  
Department of Metallurgy Engineering and Materials Science,  
IIT Indore.



## **Abstract**

As greenhouse gas emissions rise every day, developing materials that can fulfil our energy production and storage in an environment-friendly manner is crucial. Water-Splitting fuel cells and Metal-Air Batteries help solve both problems respectively. The Oxygen Reduction Reaction (ORR) and the Oxygen Evolution Reaction (OER) are both very important reactions for both of the aforementioned devices to perform desirably. In this project, the  $\text{CaFe}_x\text{Mn}_{1-x}\text{O}_3$  system was studied for  $x = 0, 0.33, 0.50, 0.67$ , and  $1$ . The optimised geometry, electronic band structure, and density of states of these materials were calculated using Density Functional Theory(DFT) implemented with the CRYSTAL17 ab-initio software package and the data was presented in a graphical and tabular manner. The obtained data can be used in follow-up work to determine whether these materials can be used as an efficient catalyst for the ORR and OER by calculating the surface energetics of these materials in a solvent environment with reaction intermediates. Of the studied materials,  $\text{CaFe}_{0.5}\text{Mn}_{0.5}\text{O}_3$  showed the most promise due to a higher occupancy in the  $e_g$  state over that in the  $t_{2g}$  state. It has a clearly defined crystal field splitting between the  $e_g$  and  $t_{2g}$  states in the d-orbitals of the transition metals Mn and Fe, and also in the overall crystal.

# Contents

	<b>Page</b>
<b>Candidate's Declaration</b>	<b>2</b>
<b>Supervisor's Certificate</b>	<b>2</b>
<b>Preface</b>	<b>4</b>
<b>Acknowledgements</b>	<b>6</b>
<b>Abstract</b>	<b>8</b>
<b>List of Figures</b>	<b>10</b>
<b>List of Tables</b>	<b>11</b>
<b>1 Literature Review</b>	<b>12</b>
1.1 Introduction . . . . .	12
1.2 Oxygen Reduction Reaction (ORR) . . . . .	13
1.3 Oxygen Evolution Reaction (OER) . . . . .	13
1.4 Why CaMnO <sub>3</sub> ? . . . . .	14
1.5 Surface Energetics Calculation . . . . .	15
<b>2 Problem Formulation and Objectives</b>	<b>16</b>
2.1 Problem Formulation . . . . .	16
2.2 Objectives . . . . .	16
<b>3 Computational Methodology</b>	<b>18</b>
3.1 Density Functional Theory . . . . .	18
3.1.1 The Schrödinger Equation . . . . .	18
3.1.2 What is a Functional? . . . . .	19
3.1.3 Kohn-Sham Equations and the Exchange Correlation Potential . . . . .	19
3.2 Computational Details . . . . .	19

<b>4 Results and Discussion</b>	<b>22</b>
4.1 Optimised Geometry and Electronic Properties . . . . .	22
4.1.1 CaMnO <sub>3</sub> . . . . .	23
4.1.2 CaFe <sub>0.33</sub> Mn <sub>0.67</sub> O <sub>3</sub> (12.5% Fe) . . . . .	25
4.1.3 CaFe <sub>0.5</sub> Mn <sub>0.5</sub> O <sub>3</sub> (25% Fe) . . . . .	27
4.1.4 CaFe <sub>0.67</sub> Mn <sub>0.33</sub> O <sub>3</sub> (37.5% Fe) . . . . .	29
4.1.5 CaFeO <sub>3</sub> . . . . .	31
4.2 Oxygen Electrocatalysis . . . . .	34
<b>5 Conclusion and Scope for Future Work</b>	<b>36</b>
5.1 Conclusion . . . . .	36
5.2 Future Work . . . . .	36

# List of Figures

3.1 Process Workflow of using the CRYSTAL17 code suite . . . . .	20
4.1 Pure CaMnO <sub>3</sub> : (a) Optimised Structure with P1 Symmetry, (b) Electronic Band Structure Diagram(left) and Density of States Plot(right) . . . . .	23
4.2 CaFe <sub>0.33</sub> Mn <sub>0.67</sub> O <sub>3</sub> (12.5% Fe): (a) Optimised Structure with P2 Symmetry, (b) Electronic Band Structure Diagram, and (c) Density of States Plot . . . . .	25
4.3 CaFe <sub>0.5</sub> Mn <sub>0.5</sub> O <sub>3</sub> (25% Fe): (a) Optimised Structure with P2 Symmetry, (b) Electronic Band Structure Diagram, and (c) Density of States Plot . . . . .	27
4.4 CaFe <sub>0.67</sub> Mn <sub>0.33</sub> O <sub>3</sub> (37.5% Fe): (a) Optimised Structure with P2 Symmetry, (b) Electronic Band Structure Diagram, and (c) Density of States Plot . . . . .	29
4.5 CaFeO <sub>3</sub> : (a) Optimised Structure with P2 Symmetry, (b) Electronic Band Structure Diagram, and (c) Density of States Plot . . . . .	31
4.6 Density of States Plot for the d-orbital for (a) Mn and (b) Fe in the 25% Fe-doped CaMnO <sub>3</sub> . [The "0" mark in the y-axis (Normalised Energy in eV) refers to the Fermi Energy of the system] . . . . .	34
4.7 Reaction Mechanisms of (a) Oxygen Reduction Reaction and (b) Oxygen Evolution Reaction. [26] Here B is the transition metal atom used in the material, i.e. Mn and Fe in our case. . . . .	35

# List of Tables

4.1 Geometry and Electronic Properties (* = Space Group) . . . . .	33
--	----

# **Chapter 1**

## **Literature Review**

### **1.1 Introduction**

The 21st Century Civilisation is entirely dependant on energy in various forms for the normal functioning of day-to-day activities. It is a well known fact that the resources for the energy are dwindling fast. The major concern is the fact that the rate of consumption of these resources is significantly higher than the rate at which they are replenished. Hence, there is a growing incentive for the development of ways to use sources of energy that are renewable. Materials development to harness these sources is thus becoming increasingly prominent in the research space for renewable energy harvesting and storage. However, experimentally determining the efficacy of all the overwhelming amount of possible kinds of materials that are possible is an expensive, labour-intensive and time-taking task and may lead to a delay in our ability to harness the renewable energy sources to our full potential. Thus, a computational approach to materials discovery is a great alternative that establishes, in theory, the efficacy of a material to perform well for harvesting energy from renewable sources. Of the many renewable sources, Hydrogen is known as a great fuel. In hydrogen fuel cells, water is split into hydrogen and oxygen electrochemically. This hydrogen is combusted with the oxygen again forming water and releasing energy whenever we need it. The water can be reused as many times as we like and the overall process is very efficient. [1] In cases when the power generated is not needed immediately or when the device is taken away from the power source, storage of this power becomes essential. Metal-air batteries can be used for this purpose. These also rely on OER and ORR, thus making electrocatalysts for these reactions is important.

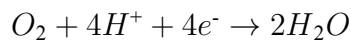
In the present work, we aim to determine the efficacy of Fe-doped CaMnO<sub>3</sub> as a bifunctional oxygen electrocatalyst. In particular, the Oxygen Reduction Reaction(ORR), and the Oxygen Evolution Reaction(OER) are of concern in this work. [2] The perovskite material, CaMnO<sub>3</sub> was specifically chosen because the mechanism with which perovskites

catalyse OER was well understood. [2] It was established that oxygen vacancies enhance the catalytic ability of  $\text{CaMnO}_3$  for the ORR in lithium-oxygen Batteries. [3, 4] However, if an oxygen atom is removed, the valency of the adjacent Manganese atoms remain unfulfilled. Addition of iron will help mitigate this issue. Also, it has been established that the thermodynamic properties of  $\text{CaMnO}_3$  are suitable for Oxygen Evolution. [5, 6] We perform the study using First-principle methods such as Hybrid Density Functional Theory using computational resources rather than performing physical experiments. This helps with providing preliminary results in a fast, cost-effective and environmentally-friendly manner.

## 1.2 Oxygen Reduction Reaction (ORR)

The Oxygen Reduction is an important reaction that occurs at the cathode and it is responsible for the formation of water that in turn generates power from the fuel cell.

The overall reduction reaction, that occurs at the cathode, is as follows: [7]



However, the actual mechanism of the reaction, especially for perovskite materials such as  $\text{CaMnO}_3$ , is quite intricate. This mechanism follows four steps, namely, displacement of hydroxide, formation of peroxide, formation of oxide, and regeneration of hydroxide. [8] All of these steps occur on the surface of the perovskite at the transition metal site. The reactions are given as follows:

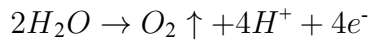
1.  $\text{CaMO}_3 - \text{OH} + \text{O}_2 + e^- \rightarrow \text{CaMO}_3 - \text{OO} + \text{OH}^-$
2.  $\text{CaMO}_3 - \text{OO} + \text{H}_2\text{O} + e^- \rightarrow \text{CaMO}_3 - \text{OOH} + \text{OH}^-$
3.  $\text{CaMO}_3 - \text{OOH} + e^- \rightarrow \text{CaMO}_3 - \text{O} + \text{OH}^-$
4.  $\text{CaMO}_3 - \text{O} + \text{H}_2\text{O} + e^- \rightarrow \text{CaMO}_3 - \text{OH} + \text{OH}^-$

M is a transition metal that occupies the B-site in the lattice, which in the current work is both Mn and Fe.

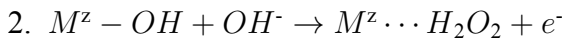
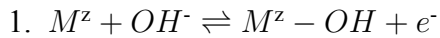
## 1.3 Oxygen Evolution Reaction (OER)

The OER is basically the reverse reaction of the ORR. It even has the exact same reaction intermediates. It is the limiting reaction in the splitting of water and hence it is essential to develop an electrochemical catalyst that will facilitate this reaction. [2]

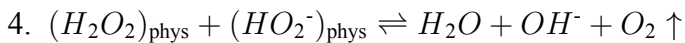
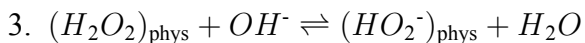
The overall oxidation reaction, that occurs at the anode, is as follows:



However, the actual mechanism of the reaction, just like for the ORR, is quite intricate, especially for perovskite materials such as  $\text{CaMnO}_3$ . This mechanism is given as follows:



The  $H_2O_2$  is physisorbed onto the  $M^z$  and the following steps occur subsequently:



Here, the  $M^z$  is a transition metal ion with the valence state  $z+$  on the surface of the perovskite. [2] In this work, the transition metal atoms are Manganese and Iron.

## 1.4 Why $\text{CaMnO}_3$ ?

It has been reported in a seemingly unrelated topic of batteries that use ion transport as the primary mechanism of charge transport, that, the catalytic ability of  $\text{CaMnO}_3$  is very good. When oxygen vacancies are introduced in the lattice, this is enhanced significantly. [3, 4]

This is the motivation for our study of the efficacy of this catalyst in water splitting applications. Since the oxygen evolution reaction is the rate determining step of the water splitting process, a suitable catalyst must be developed for kinetically feasible and efficient water splitting to occur. Same goes with Metal-air batteries and for the ORR in both applications.

It has been established that oxygen deficiency in the  $\text{CaMnO}_3$  lattice facilitates the catalytic activity. [3, 4] However, by removing oxygen atoms, the valency of the manganese atoms will be unsatisfied. Hence, replacing manganese with iron will ensure a stoichiometric solid with no free bonds. Thus, Fe-doped  $\text{CaMnO}_3$  is a material that must be studied as it holds tremendous potential of becoming a strong catalyst for the OER.

## 1.5 Surface Energetics Calculation

To determine the activity of the material for the ORR/OER, the free energy change of each reaction step must be calculated, and the overall free energy must be negative. This can be performed using a computational model suggested by Nørskov et al. [9] This method is interesting as the relative free energy is affected by the potential difference through the chemical potential of the electrons in the hydrogen electrode. As the reaction intermediates for both the OER and ORR are the same (as we are not involving lattice oxygen participation in the OER in this study), all calculation methods will be similar for both processes. Gibbs Free Energy is calculated by converting the binding energies calculated using DFT ( $\Delta E$ ) by adding entropic ( $T\Delta S$ ) and zero-point energy ( $\Delta ZPE$ ) corrections. Thus, we get,

$$\Delta G = \Delta E + \Delta ZPE - T\Delta S + \Delta G_\phi$$

ZPE corrections and entropies of the ORR/OER intermediates are calculated from the vibrational frequencies according to standard methods, and those of the gas-phase molecules are obtained from thermodynamics databases.  $\Delta G_\phi$  is the effect of electrode potential which is applied by shifting the free energy change  $\Delta G$  by  $\Delta G_\phi = e\phi$ , where  $e$  is the elementary charge and  $\phi$  is the potential difference between electrode and counter electrode (versus reversible hydrogen electrode, RHE). The equilibrium potential  $\phi_{eq}$  corresponds to zero net reaction free energy ( $G_1+G_2+G_3+G_4 = 2\Delta G_W + 4e\phi = 0$ ) of the overall ORR process, thus, we have  $\phi_{eq} = \frac{-\Delta G_W}{2e}$ , where  $\Delta G_W = G(H_2O) - G(H_2) - \frac{G(O_2)}{2}$  is the free energy of formation of water from 1 mol H<sub>2</sub> and  $\frac{1}{2}$  mol O<sub>2</sub>. The ORR potential  $\phi_{ORR}$  corresponds to the highest potential  $\phi$  at which all steps along the reaction decrease the free energy. The theoretical ORR overpotential is then calculated by  $\eta = \phi_{eq} - \phi_{ORR}$ . The same procedure is, of course, also employed for the OER, taking into account the reverse mechanism. The effect of water on the ORR activity is an important factor to take into account. This can be done by employing a solvation correction to ORR/OER intermediates because reactions occur in the presence of water in electrolytes. [7] A study of platinum-catalyzed ORR using the Poisson– Boltzmann implicit continuum model has been done earlier [10] and the solvation correction can be taken from this. The solvation correction energies for the OO\*, O\*, HO\*, and HOO\* intermediates, are −0.32, −0.47, −0.75, and −0.54 eV, respectively.

# **Chapter 2**

## **Problem Formulation and Objectives**

### **2.1 Problem Formulation**

Oxygen electrocatalysis is crucial for the water splitting to occur in a fuel cell as it is the Rate Limiting Step of the entire process. It is also crucial in metal-air batteries. Thus, it is important that a material that possesses good catalytic ability for this reaction to occur at the working temperature (usually room temperature). [2]

In the current work, Fe-doped  $\text{CaMnO}_3$ , a material that could potentially have such an ability is studied to confirm its suitability to this application. This is determined using first-principle methods such as Hybrid Density Functional Theory.

The geometry of the lattice structure of the material is to be optimised using ab-initio based code suite CRYSTAL17 using the Hybrid B3LYP Density Functional Theory method and the TZVP Gaussian type basis sets. [11, 12, 13, 14, 15] The parameters of this optimised structure are to be used to determine the electronic band structure and density of states of the material. This information can be used to figure out the  $e_g$  filling of the d orbital in the transition metals Mn and Fe.

Once these are deemed satisfactory, the reaction pathway is to be simulated as given in sections 1.2 and 1.3 . The free energy changes of each step are calculated, from which the net free energy change can be determined. This will ultimately decide whether or not the material is useful as a catalyst for the oxygen evolution reaction.

### **2.2 Objectives**

1. Optimize geometry, and calculate Electronic Band Structure and Density of States of pure  $\text{CaMnO}_3$  without any defects and dopants.
2. Optimize geometry, and calculate Electronic Band Structure and Density of States of Fe-doped  $\text{CaMnO}_3$  at different doping concentrations.

3. Calculate reaction intermediate energies from reaction pathway as given in sections 1.2 and 1.3 and calculate the overall free energy change in the ORR and OER for certain doping amounts of Fe in  $\text{CaMnO}_3$ . If the reaction is not feasible with this material, then other dopant and vacancy concentrations will be tried, and the process will be repeated.

# Chapter 3

## Computational Methodology

### 3.1 Density Functional Theory

To calculate all of the electronic properties and surface energy in all the materials studied, we have employed the use of Density Functional Theory. The aim of this section is to explain what Density Functional Theory is and how it was used in our work.

#### 3.1.1 The Schrödinger Equation

To calculate all properties, we require the solutions to the Schrödinger Equation. This equation, in the time independent, nonrelativistic, Born-Oppenheimer approximation is:

$$\hat{H}\Psi(\mathbf{r}_1, \mathbf{r}_2, \dots, \mathbf{r}_N) = E(\mathbf{r}_1, \mathbf{r}_2, \dots, \mathbf{r}_N)$$

The Hamiltonian operator,  $\hat{H}$ , consists of a sum of three terms; the kinetic energy, the interaction with the external potential ( $V_{ext}$ ) and the electron-electron interaction ( $V_{ee}$ ). That is;

$$\hat{H} = -\frac{1}{2} \sum_i^N \nabla_i^2 + V_{ext} + \sum_{i < j}^N \frac{1}{|\mathbf{r}_i - \mathbf{r}_j|}$$

In materials simulation the external potential of interest is simply the Coulomb interaction of the electrons with the atomic nuclei.

From this, it can be seen that the total energy 'E' can be written as:

$$E[\rho] = T[\rho] + V_{ext}[\rho] + V_{ee}[\rho]$$

This is called the energy functional.

### 3.1.2 What is a Functional?

A Functional is like a black box into which if we input a function, we get a number out.  
Ex: Definite Integral:

$$\int_0^1 x^2 dx \approx 0.33$$

$$\int_0^1 \cos x dx \approx 0.84$$

It can be seen above that in both the given examples while the limits of integration are the same, the number that we get in both cases changed because of the function changed. Here, the integral itself is the functional and the function that we are integrating is the input to the functional, while the number we get is the output.

In Density Functional Theory, we input the Wave Function of the electrons in the material (Basis Set) into an Electron Density Functional and this gives us the electronic properties of the materials.

### 3.1.3 Kohn-Sham Equations and the Exchange Correlation Potential

The breakthrough here was the fact that Kohn and Sham showed that the potential in a material with all electrons interacting with each other can be written as a sum of the Coulomb potential and the Exchange-Correlation(XC) Functional. This simplified the problem to a great extent and allowed for the computation of the Schrödinger Equation to determine electronic properties.

Thus, the energy functional can be written as:

$$E[\rho] = T_S[\rho] + V_{ext}[\rho] + V_H[\rho] + E_{xc}[\rho]$$

So,

$$E_{xc}[\rho] = (T[\rho] - T_S[\rho]) + (V_{ee}[\rho] - V_H[\rho])$$

It is this Exchange Correlation potential that is our Density Functional. It is only a function of the Electron Density within a material.

## 3.2 Computational Details

The B3LYP method [12, 13, 14, 15] was applied for Geometry optimisation, Wave Function Optimisation, and One electron Properties such as electronic band structure and Density of States. All of these properties were calculated for pristine CaMnO<sub>3</sub>, iron-doped CaMnO<sub>3</sub> at three amounts of doping (12.5%, 25%, and 37.5%), and pristine CaFeO<sub>3</sub>, implemented in the CRYSTAL17 code using the same level of theory with the same basis

sets in each case. [16] All the computational calculations were carried out using triple zeta valence with polarization (TZVP) quality Gaussian type basis sets for all Ca, Mn, Fe, and O atoms. [11] The B3LYP method is a first principles based hybrid periodic unrestricted Density Functional Theory method and it is very effective for calculations related to materials, such as the electronic structure, geometry, electronic properties, etc. GGA or hybrid functionals, which are unrestricted Density Functional Theory methods, are not affected by the phenomenon of spin contamination as much as the Hartree–Fock (HF) theory, and thus, are better suited for studies of this sort. [17, 18, 19]

The electron integration was performed on 4x4x4 Pack-Monkhorst type of k-point sampling[20], and the SCF convergence criteria was set to  $10^{-7} Ha$  for at most 800 cycles.

The detailed process workflow when using the CRYSTAL17 software is given in the figure 3.1, and it is very similar to an earlier work performed by N. Sinha et al. [17]

Visualization for Electronic and Structural Analysis (VESTA) [21] and Materials Studio software were used for visualization and representation of all models from the Crystallographic Information files that were made using the optimised geometric parameters of each system.

## Process Workflow

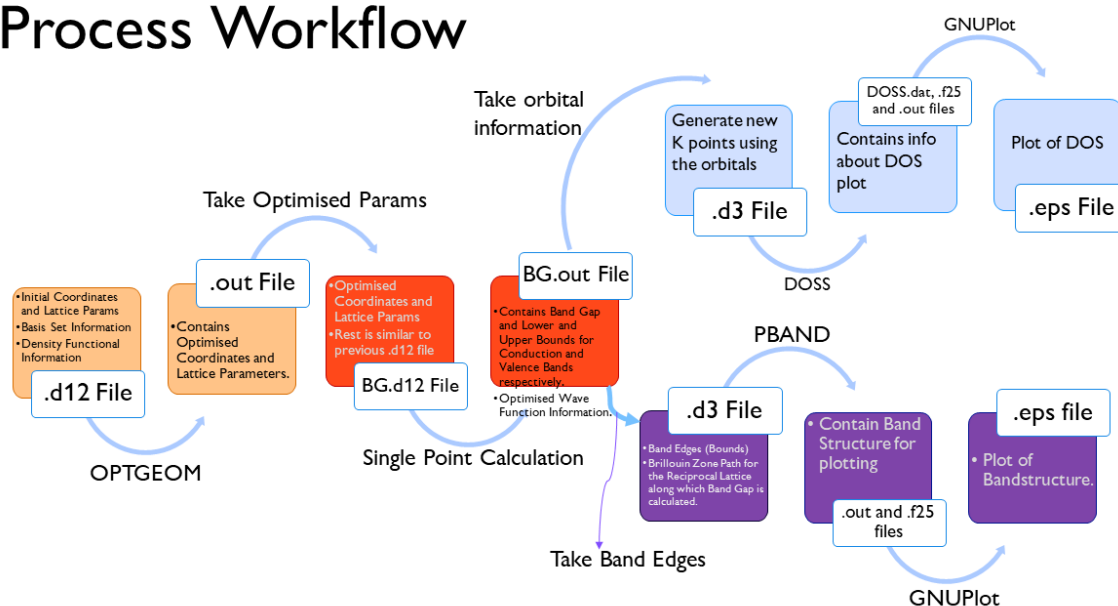


Figure 3.1: Process Workflow of using the CRYSTAL17 code suite



# Chapter 4

## Results and Discussion

### 4.1 Optimised Geometry and Electronic Properties

Geometry optimisation, Wave Function Optimisation, and One electron Properties such as electronic band structure and Density of States were calculated for pristine CaMnO<sub>3</sub>, iron-doped CaMnO<sub>3</sub> at three amounts of doping (12.5%, 25%, and 37.5%), and pristine CaFeO<sub>3</sub>, implemented in the CRYSTAL17 code using the same level of theory with the same basis sets in each case. [16] All the computational calculations were carried out using triple zeta valence with polarization (TZVP) quality Gaussian type basis sets for all Ca, Mn, Fe, and O atoms. [11] For this, the B3LYP method [12, 13, 14, 15] was applied. The B3LYP method is a first principles based hybrid periodic unrestricted Density Functional Theory method and it is very effective for calculations related to materials, such as the electronic structure, geometry, electronic properties, etc. GGA or hybrid functionals, which are unrestricted Density Functional Theory methods, are not affected by the phenomenon of spin contamination as much as the Hartree–Fock (HF) theory, and thus, are better suited for studies of this sort. [17]

The electron integration was performed on 4x4x4 Pack-Monkhorst type of k-point sampling[20], and the SCF convergence criteria was set to  $10^{-7} Ha$  for at most 800 cycles.

### 4.1.1 CaMnO<sub>3</sub>

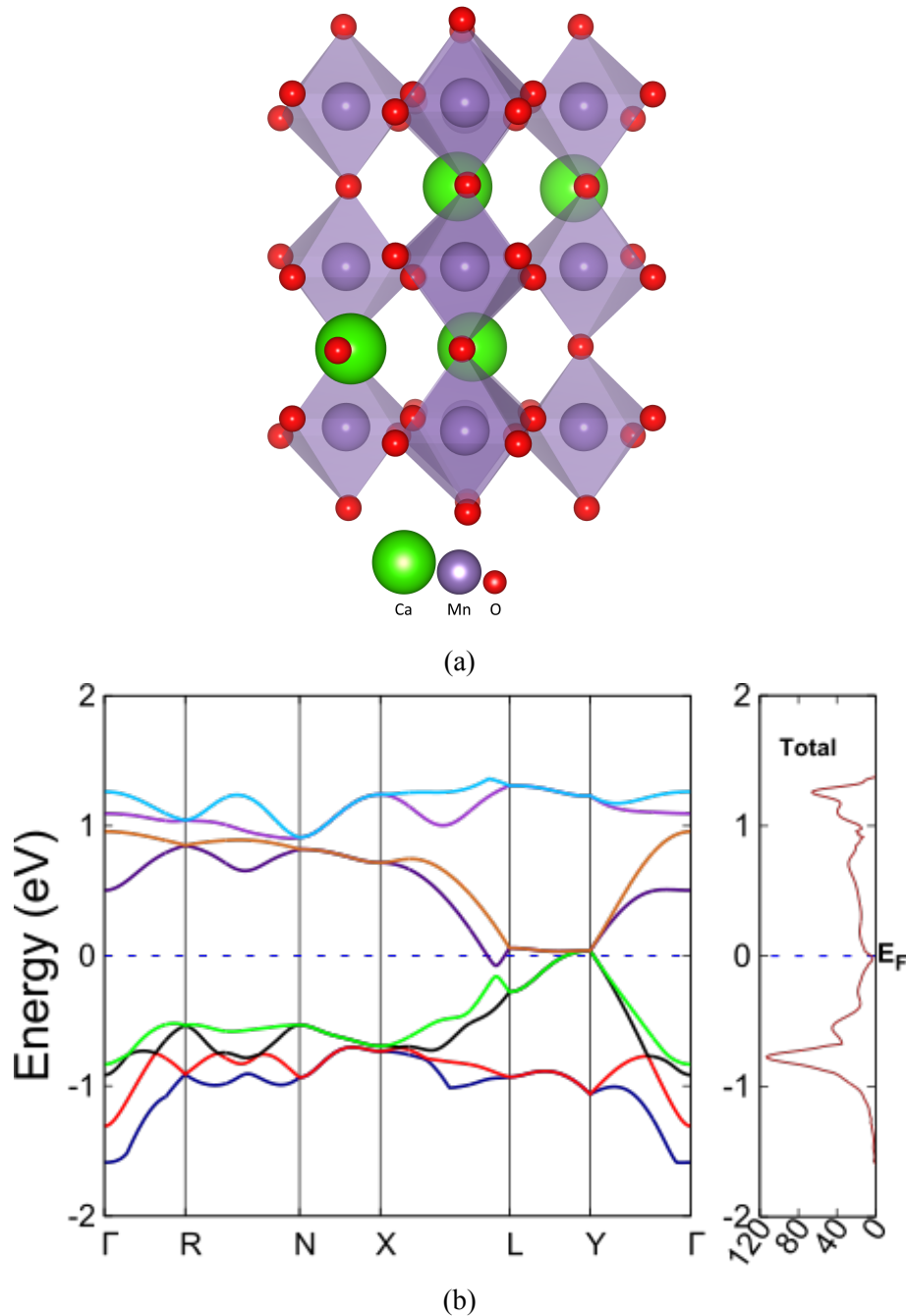


Figure 4.1: Pure CaMnO<sub>3</sub>: (a) Optimised Structure with P1 Symmetry, (b) Electronic Band Structure Diagram(left) and Density of States Plot(right)

### DFT Details and Geometry Optimisation

The ab initio based CRYSTAL17 code [16] was used for optimisation the geometry of the Pristine CaMnO<sub>3</sub>. It was optimised using the triple zeta valence with polarization (TZVP) quality Gaussian basis sets for the Ca, Mn, and O atoms [11]. To perform accurate calculation of the optimised geometry, the unrestricted DFT method, B3LYP, was employed. [12, 13, 14, 15]

The crystal structure for this material with the optimized geometry can be seen in Fig.4.1a. This material has an orthorhombic distortion of (0.996, 1.046).

### One-Electron Properties

Once the equilibrium crystal structure has been calculated, the electronic properties, such as electronic band structure and density of states, have been calculated at the same level of theory, i.e., the B3LYP DFT method using the CRYSTAL17 code. The symmetry points  $\Gamma$ -R-N-X-L-Y- $\Gamma$  were employed in evaluating the band structure as they were in agreement with the symmetry of this crystal structure (P1). [22, 23]

The valence band and conduction band in this material overlap and hence the material is conducting and thus is not useful for the purpose of water splitting.

The Electronic Band Structure Diagram for pristine CaMnO<sub>3</sub> is shown in Fig. 4.1b(left).

The Density of States was also calculated and the plot is shown in Fig. 4.1b(right). It can also be seen that from the DOS plot that there is no separation between the e<sub>g</sub> and t<sub>2g</sub> orbital occupancies, thus suggesting less Crystal Field Splitting for that system. [24]

### 4.1.2 $\text{CaFe}_{0.33}\text{Mn}_{0.67}\text{O}_3$ (12.5% Fe)

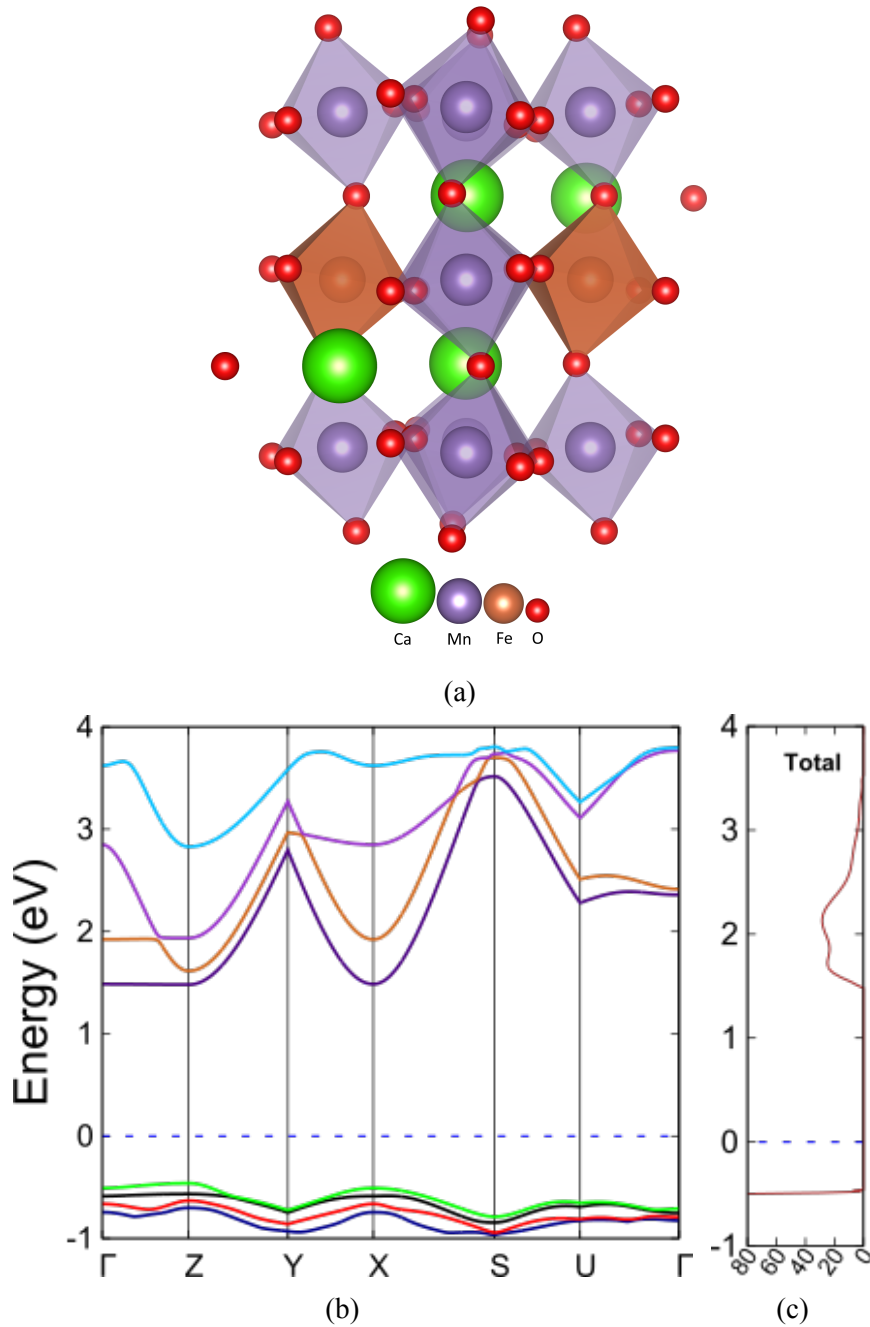


Figure 4.2:  $\text{CaFe}_{0.33}\text{Mn}_{0.67}\text{O}_3$  (12.5% Fe): (a) Optimised Structure with P2 Symmetry, (b) Electronic Band Structure Diagram, and (c) Density of States Plot

### DFT Details and Geometry Optimisation

The ab initio based CRYSTAL17 code [16] was used for optimisation the geometry of 12.5% Fe-doped  $\text{CaMnO}_3$  ( $\text{CaFe}_{0.33}\text{Mn}_{0.67}\text{O}_3$ ). It was optimised using the triple zeta valence with polarization (TZVP) quality Gaussian basis sets for the Ca, Mn, Fe, and O atoms [11]. To perform accurate calculation of the optimised geometry, the unrestricted DFT method, B3LYP, was employed. [12, 13, 14, 15]

The crystal structure for this material with the optimized geometry with a P2 symmetry can be seen in Fig.4.2a.

This material has an orthorhombic distortion of (0.994, 1.007).

### One-Electron Properties

Once the equilibrium crystal structure has been calculated, the electronic properties, such as electronic band structure and density of states, have been calculated at the same level of theory, i.e., the B3LYP DFT method using the CRYSTAL17 code. The symmetry points  $\Gamma$ -Z-Y-X-S-U- $\Gamma$  were employed in evaluating the band structure as they were in agreement with the symmetry of this crystal structure (P2). [22, 23]

As can be seen in the Fig.4.2b, the band gap has been calculated to be a Direct Band Gap of 1.9401 eV for the Alpha electrons.

The Density of States was also calculated and the plot is shown in Fig.4.2c.

It can also be seen from the Density of States plot 4.2c that there is a lot of separation between the  $e_g$  and  $t_{2g}$  orbital occupancies, thus suggesting a good Crystal Field Splitting for that system. This indicates this might be a promising candidate for the ORR/OER as it indicates a relatively high average occupancy of the  $e_g$  state. It is the covalency and interaction of  $e_g$  of the d-orbital of the transition metals and the p-band centre of the Oxygen in the intermediate that is a descriptor of the catalytic activity of the material. [24]

### 4.1.3 CaFe<sub>0.5</sub>Mn<sub>0.5</sub>O<sub>3</sub> (25% Fe)

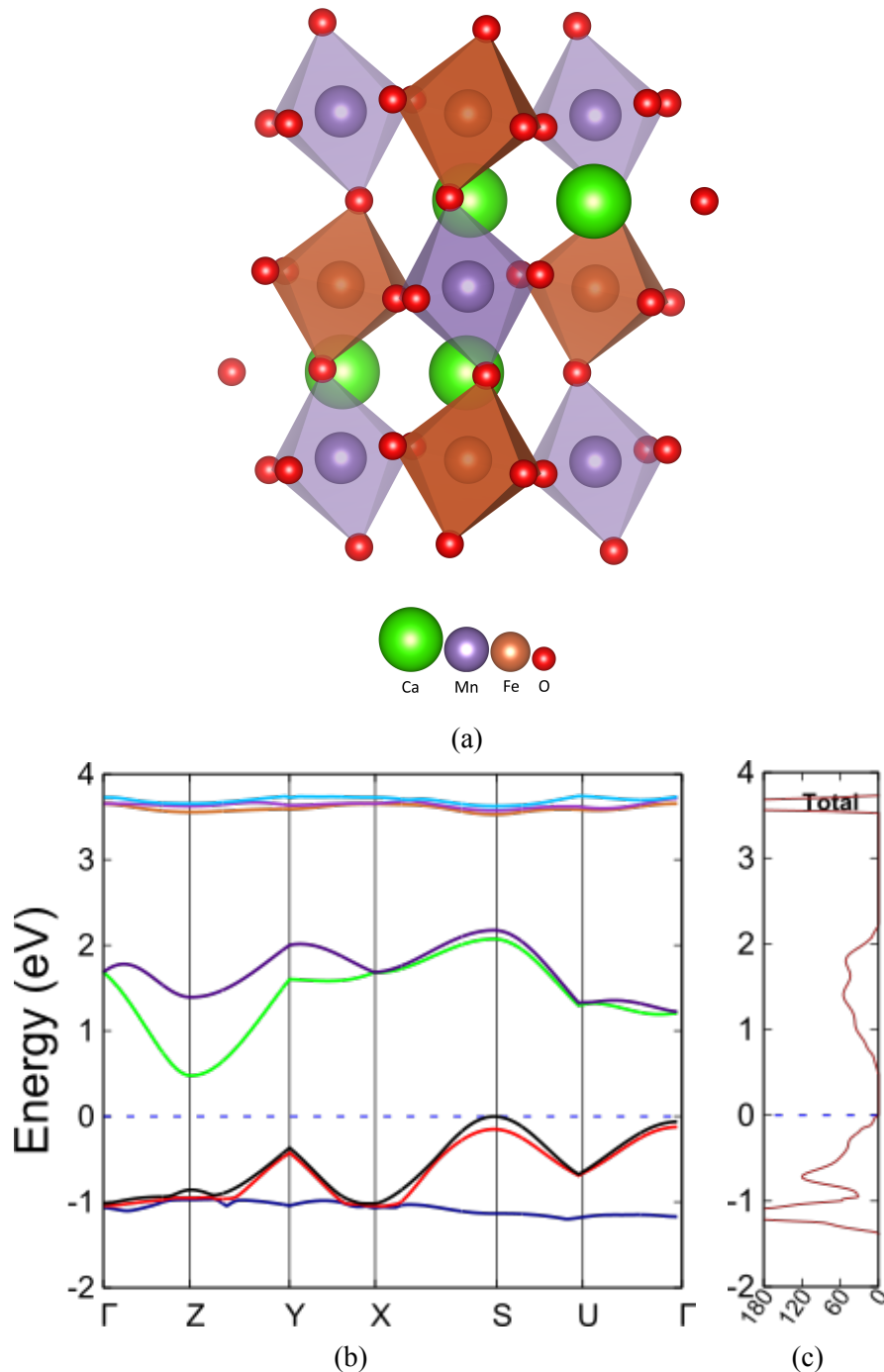


Figure 4.3: CaFe<sub>0.5</sub>Mn<sub>0.5</sub>O<sub>3</sub> (25% Fe): (a) Optimised Structure with P2 Symmetry, (b) Electronic Band Structure Diagram, and (c) Density of States Plot

### DFT Details and Geometry Optimisation

The ab initio based CRYSTAL17 code [16] was used for optimisation the geometry of 25% Fe-doped  $\text{CaMnO}_3$  ( $\text{CaFe}_{0.5}\text{Mn}_{0.5}\text{O}_3$ ). It was optimised using the triple zeta valence with polarization (TZVP) quality Gaussian basis sets for the Ca, Mn, Fe, and O atoms [11]. To perform accurate calculation of the optimised geometry, the unrestricted DFT method, B3LYP, was employed. [12, 13, 14, 15]

The crystal structure for this material with the optimized geometry with a P2 symmetry can be seen in Fig.4.3a.

This material has an orthorhombic distortion of (0.994, 1.036).

### One-Electron Properties

Once the equilibrium crystal structure has been calculated, the electronic properties, such as electronic band structure and density of states, have been calculated at the same level of theory, i.e., the B3LYP DFT method using the CRYSTAL17 code. The symmetry points  $\Gamma$ -Z-Y-X-S-U- $\Gamma$  were employed in evaluating the band structure as they were in agreement with the symmetry of this crystal structure (P2). [22, 23]

As can be seen in the Fig.4.3b, the band gap has been calculated to be an Indirect Band Gap of 0.48eV for the Alpha electrons.

The Density of States was also calculated and the plot is shown in Fig.4.3c.

It can also be seen from the Density of States plot 4.2c that there is a lot of separation between the  $e_g$  and  $t_{2g}$  orbital occupancies, thus suggesting a good Crystal Field Splitting for that system. This indicates this might be a promising candidate for the ORR/OER as it indicates a relatively high average occupancy of the  $e_g$  state. It is the covalency and interaction of  $e_g$  of the d-orbital of the transition metals and the p-band centre of the Oxygen in the intermediate that is a descriptor of the catalytic activity of the material. [24]

#### 4.1.4 CaFe<sub>0.67</sub>Mn<sub>0.33</sub>O<sub>3</sub> (37.5% Fe)

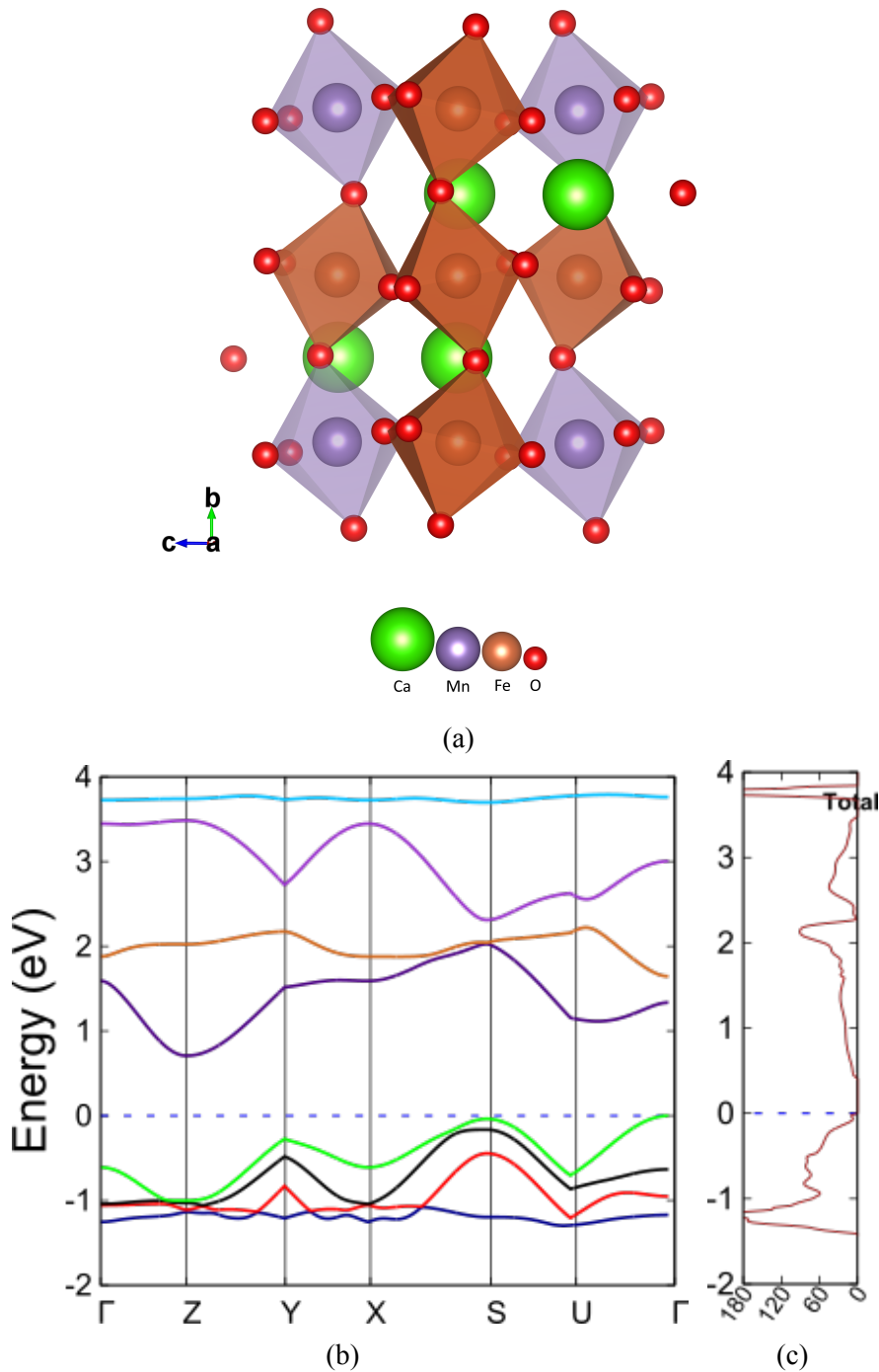


Figure 4.4: CaFe<sub>0.67</sub>Mn<sub>0.33</sub>O<sub>3</sub> (37.5% Fe): (a) Optimised Structure with P2 Symmetry, (b) Electronic Band Structure Diagram, and (c) Density of States Plot

### DFT Details and Geometry Optimisation

The ab initio based CRYSTAL17 code [16] was used for optimisation the geometry of 37.5% Fe-doped  $\text{CaMnO}_3$  ( $\text{CaFe}_{0.67}\text{Mn}_{0.33}\text{O}_3$ ). It was optimised using the triple zeta valence with polarization (TZVP) quality Gaussian basis sets for the Ca, Mn, Fe, and O atoms [11]. To perform accurate calculation of the optimised geometry, the unrestricted DFT method, B3LYP, was employed. [12, 13, 14, 15]

The crystal structure for this material with the optimized geometry with a P2 symmetry can be seen in Fig.4.4a.

This material has an orthorhombic distortion of (0.998, 1.025).

### One-Electron Properties

Once the equilibrium crystal structure has been calculated, the electronic properties, such as electronic band structure and density of states, have been calculated at the same level of theory, i.e., the B3LYP DFT method using the CRYSTAL17 code. The symmetry points  $\Gamma$ -Z-Y-X-S-U- $\Gamma$  were employed in evaluating the band structure as they were in agreement with the symmetry of this crystal structure (P2). [22, 23]

As can be seen in the Fig.4.4b, the band gap has been calculated to be an Indirect Band Gap of 0.45eV for the Alpha electrons.

The Density of States was also calculated and the plot is shown in Fig.4.4c.

It can also be seen from the Density of States plot 4.4c that there is a small amount of separation between the  $e_g$  and  $t_{2g}$  orbital occupancies, thus suggesting some amount of Crystal Field Splitting for that system. This indicates this might be a promising candidate for the ORR/OER as it indicates a relatively higher average occupancy of the  $e_g$  state. It is the covalency and interaction of  $e_g$  of the d-orbital of the transition metals and the p-band centre of the Oxygen in the intermediate that is a descriptor of the catalytic activity of the material. [24]

#### 4.1.5 CaFeO<sub>3</sub>

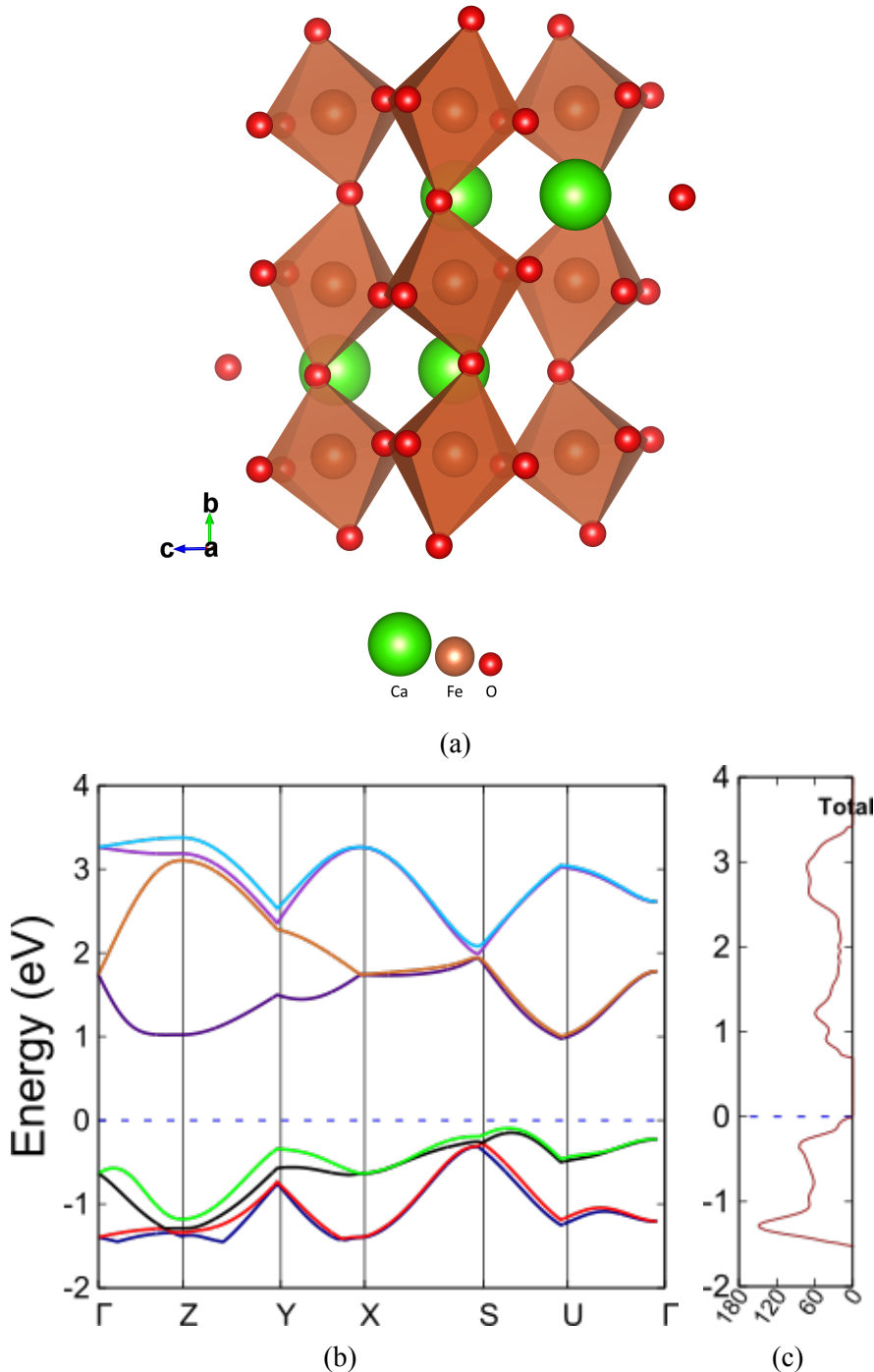


Figure 4.5: CaFeO<sub>3</sub>: (a) Optimised Structure with P2 Symmetry, (b) Electronic Band Structure Diagram, and (c) Density of States Plot

### DFT Details and Geometry Optimisation

The ab initio based CRYSTAL17 code [16] was used for optimisation the geometry of Pristine CaFeO<sub>3</sub>. It was optimised using the triple zeta valence with polarization (TZVP) quality Gaussian basis sets for the Ca, Mn, Fe, and O atoms [11]. To perform accurate calculation of the optimised geometry, the unrestricted DFT method, B3LYP, was employed. [12, 13, 14, 15]

The crystal structure for this material with the optimized geometry with a P2 symmetry can be seen in Fig.4.5a.

This material has an orthorhombic distortion of (1.006, 0.999).

### One-Electron Properties

Once the equilibrium crystal structure has been calculated, the electronic properties, such as electronic band structure and density of states, have been calculated at the same level of theory, i.e., the B3LYP DFT method using the CRYSTAL17 code. The symmetry points  $\Gamma$ -Z-Y-X-S-U- $\Gamma$  were employed in evaluating the band structure as they were in agreement with the symmetry of this crystal structure (P2). [22, 23]

The band gap in this material is 0.75eV and it is indirect. The Electronic Band Structure Diagram for pristine CaFeO<sub>3</sub> is shown in Fig. 4.5b.

The Density of States was also calculated and the plot is shown in Fig. 4.5c.

It can also be seen from the Density of States plot 4.5c that there is a separation between the e<sub>g</sub> and t<sub>2g</sub> orbital occupancies, thus suggesting some amount of Crystal Field Splitting for that system. This indicates this might be a promising candidate for the ORR/OER as it indicates a relatively higher average occupancy of the e<sub>g</sub> state. It is the covalency and interaction of e<sub>g</sub> of the d-orbital of the transition metals and the p-band centre of the Oxygen in the intermediate that is a descriptor of the catalytic activity of the material. [24]

## Geometry and Electronic Properties Data summarised

Property	Fe-Doped CaMnO <sub>3</sub>				
	CaMnO <sub>3</sub>	12.5% Fe	25% Fe	37.5% Fe	CaFeO <sub>3</sub>
a	5.38Å	5.28Å	5.37Å	5.36Å	5.31Å
b	7.25Å	7.37Å	7.29Å	7.38Å	7.56Å
c	5.36Å	5.25Å	5.34Å	5.35Å	5.34Å
α	90°	89.85°	89.17°	89.49°	90.93°
β	90°	90.01°	89.99°	91.56°	89.99°
γ	90°	90.08°	89.99°	90.61°	89.99°
Symmetry	P1 (1*)	P2 (2*)	P2 (2*)	P2 (2*)	P2 (2*)
Band Gap	Conducting	1.94eV	0.48eV	0.45eV	0.75eV
Band Gap Type	Conducting	Direct	Indirect	Indirect	Indirect
Orthorhombic Distortion ( $\frac{c}{a}, \frac{\sqrt{2}c}{b}$ )	(0.996, 1.046)	(0.994, 1.007)	(0.994, 1.036)	(0.998, 1.025)	(1.006, 0.999)

Table 4.1: Geometry and Electronic Properties (\* = Space Group)

As can be seen in table 4.1, the lattice parameters stay roughly the same in all three dimensions, in all dopant concentrations. It varies the least in the 'c' parameter and the most in the 'b' parameter.

Bond angles show a similar trend.

It can be observed that the lattice has an orthorhombic distortion ( $\frac{c}{a}, \frac{\sqrt{2}c}{b}$ ) as has been confirmed from previous studies on the system. [25] This distortion does not show any clear trend across all systems, but no crystal shows perfect orthorhombic structure.

While the undoped structure that was studied was unsymmetrized (P1), all concentrations of dopant Fe were symmetrised with the P2 symmetry.

The band gap did not show a monotonous trend with increasing dopant concentration. Without any dopant, it was conducting (0eV band gap), and it spiked at 1.94eV at 12.5% doping. It decreased sharply to 0.48eV at 25% doping and remained about the same at 37.5% doping at 0.45eV. It rose to 0.75eV at 50% doping where there was no Mn in the lattice at all. The largest band gap, i.e. 1.94eV at 12.5% doping, was the only direct band gap that was observed. All other doped structures had indirect band gaps, including pristine CaFeO<sub>3</sub>, while the pristine CaMnO<sub>3</sub> structure was conducting.

## 4.2 Oxygen Electrocatalysis

### d-orbital DOS of Mn and Fe in $\text{CaFe}_{0.5}\text{Mn}_{0.5}\text{O}_3$

From the Density of States(DOS) Plots that we have seen so far for the Pristine  $\text{CaMnO}_3$  and  $\text{CaFeO}_3$ , and the former doped with three different concentrations of Fe, the system with 25% has shown a good separation of the  $e_g$  and  $t_{2g}$  orbital occupancy. Below are shown the Density of States plots of the d-orbital of Mn(4.6a) and Fe(4.6b) in the 25% Fe-doped  $\text{CaMnO}_3$ .

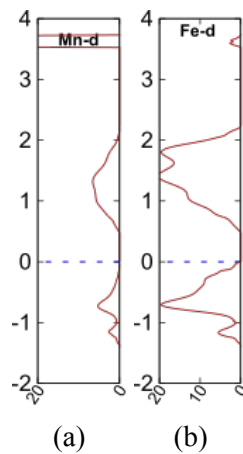


Figure 4.6: Density of States Plot for the d-orbital for (a) Mn and (b) Fe in the 25% Fe-doped  $\text{CaMnO}_3$ . [The "0" mark in the y-axis (Normalised Energy in eV) refers to the Fermi Energy of the system]

From these plots, it can be seen that there is a good amount of separation between the occupancy  $e_g$  and  $t_{2g}$  orbitals, thus suggesting a good Crystal Field Splitting for that system. Importantly, there is higher occupancy in the  $e_g$  state than  $t_{2g}$  state in the d-orbitals of both of the transition metals. The actual calculation of the  $e_g$  filling has not been able to be performed because of the delays due the ongoing pandemic, however the above system looks promising. [24, 7]

### Surface Energetics

To determine the catalytic activity of the material in question for the ORR/OER, the binding energy must be calculated for each ORR/OER intermediate (as given in Figs. 4.7a and 4.7b) on the  $\text{CaFe}_x\text{Mn}_{1-x}\text{O}_3$  surface. This is being calculated using the B3LYP level of DFT theory, thus the energy that will be calculated is a DFT Binding energy. These binding energies will be calculated according to the equation:

$$\Delta E_{\text{adsorbate}} = E_{\text{CaFe}_x\text{Mn}_{1-x}\text{O}_3-\text{adsorbate}} - E_{\text{CaFe}_x\text{Mn}_{1-x}\text{O}_3} - E_{\text{adsorbate}}$$

, where  $E_{\text{CaFe}_x\text{Mn}_{1-x}\text{O}_3-\text{adsorbate}}$ ,  $E_{\text{CaFe}_x\text{Mn}_{1-x}\text{O}_3}$ , and  $E_{\text{adsorbate}}$  are the energies of the surface with adsorbed intermediate, the bare surface, and the isolated ORR/OER intermediate, respec-

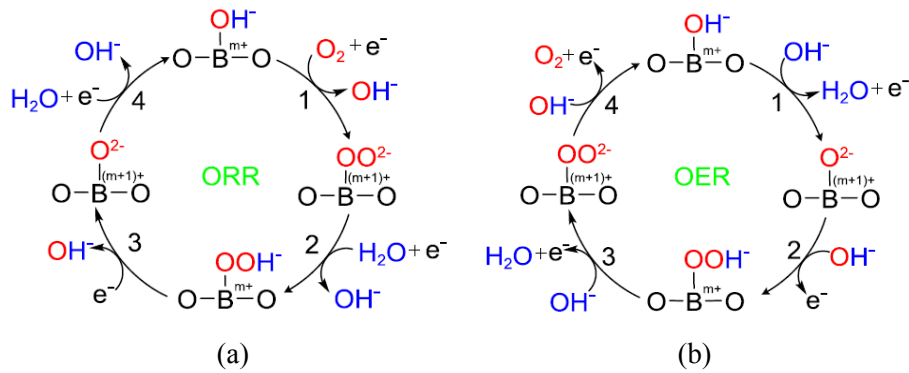


Figure 4.7: Reaction Mechanisms of (a) Oxygen Reduction Reaction and (b) Oxygen Evolution Reaction. [26] Here B is the transition metal atom used in the material, i.e. Mn and Fe in our case.

tively. The negative sign of  $E_{adsorbate}$  corresponds to energy gain of the system due to adsorption of the ORR intermediate, and the more negative the  $E_{adsorbate}$  value, the stronger is the chemical interaction between the adsorbate and the surface.[8] Any other corrections from the reference energies of  $O_2$  for the DFT method used can be made.

# **Chapter 5**

## **Conclusion and Scope for Future Work**

### **5.1 Conclusion**

From the electronic structure properties obtained from the optimised structures of the five systems that we have studied, we get the information that could help us make a guess about the efficacy of two of the systems as oxygen electrocatalyst.

Due to the wide separation between the  $e_g$  and  $t_{2g}$  orbital occupancies for two of the five systems studied, i.e. 12.5% Fe-doped  $\text{CaMnO}_3$  and 25% Fe-doped  $\text{CaMnO}_3$ , we can be optimistic that there is a possibility that there is a good amount( $\approx 1$ ) of  $e_g$  filling.

If this is confirmed, along with the calculation of the surface energetics, it can be ascertained whether doping Fe in  $\text{CaMnO}_3$  improves its efficacy as an oxygen electrocatalyst.

### **5.2 Future Work**

Now that the Electronic Band Structure and the Density of States of the various concentrations of Fe doped in  $\text{CaMnO}_3$  have been calculated, we can proceed to the next step of the study. Some of these show promise as potential candidates for an electrocatalyst for the ORR/OER.

However, to establish this as a fact, the reaction pathway must be simulated and the free energies corresponding to each reaction must be calculated. The reaction pathway is similar to that described in sections 1.2 and 1.3.

In this reaction pathway, if the net free energy is not negative or not low enough for kinetically adequate Oxygen Evolution Reaction (OER) to occur, then the entire process must be repeated for a different doping location of Fe per concentration, and the corre-

sponding properties will be studied to ascertain these materials as suitable electrochemical catalysts for the oxygen evolution reaction.

Due to the delays caused by the ongoing pandemic, this data will not have been calculated by the time this report is submitted. However, it is hoped that this data might be published in the future.

In this study, the advantage gained by introducing a species with a different valency in the B-site was not utilised. The oxygen vacancies created by the doping the doping of iron with 2+ valency rather than 3+ would have created opportunity for adsorption of the oxygen containing intermediates and this could have drastically improved the performance of this perovskite oxide as an oxygen catalyst. In the future this can be studied.

# References

- [1] Jiajia Song et al. “A review on fundamentals for designing oxygen evolution electrocatalysts”. In: *Chem. Soc. Rev.* 49 (7 2020), pp. 2196–2214. DOI: 10.1039/C9CS00607A. URL: <http://dx.doi.org/10.1039/C9CS00607A>.
- [2] John O’M. Bockris and Takaaki Otagawa. “Mechanism of oxygen evolution on perovskites”. In: *The Journal of Physical Chemistry* 87.15 (1983), pp. 2960–2971. DOI: 10.1021/j100238a048. eprint: <https://doi.org/10.1021/j100238a048>. URL: <https://doi.org/10.1021/j100238a048>.
- [3] Guruprasad S. Hegde et al. “Role of Defects in Low-Cost Perovskite Catalysts toward ORR and OER in Lithium–Oxygen Batteries”. In: *ACS Applied Energy Materials* 3.2 (2020), pp. 1338–1348. DOI: 10.1021/acsaem.9b01727. eprint: <https://doi.org/10.1021/acsaem.9b01727>. URL: <https://doi.org/10.1021/acsaem.9b01727>.
- [4] Dong Un Lee et al. “Highly active Co-doped LaMnO<sub>3</sub> perovskite oxide and N-doped carbon nanotube hybrid bi-functional catalyst for rechargeable zinc–air batteries”. In: *Electrochemistry Communications* 60 (2015), pp. 38–41. ISSN: 1388-2481. DOI: <https://doi.org/10.1016/j.elecom.2015.08.001>. URL: <https://www.sciencedirect.com/science/article/pii/S1388248115002118>.
- [5] Emanuela Mastronardo et al. “The favourable thermodynamic properties of Fe-doped CaMnO<sub>3</sub> for thermochemical heat storage”. In: *J. Mater. Chem. A* 8 (17 2020), pp. 8503–8517. DOI: 10.1039/DOTA02031A. URL: <http://dx.doi.org/10.1039/DOTA02031A>.
- [6] Emanuela Mastronardo et al. “Fe-doped CaMnO<sub>3</sub> for thermochemical heat storage application”. In: *AIP Conference Proceedings* 2126.1 (2019), p. 210005. DOI: 10.1063/1.5117754. eprint: <https://aip.scitation.org/doi/pdf/10.1063/1.5117754>. URL: <https://aip.scitation.org/doi/abs/10.1063/1.5117754>.
- [7] Jin Suntivich et al. “Design principles for oxygen-reduction activity on perovskite oxide catalysts for fuel cells and metal–air batteries”. In: *Nature Chemistry* 3.7 (July

- 2011), pp. 546–550. ISSN: 1755-4349. DOI: 10.1038/nchem.1069. URL: <https://doi.org/10.1038/nchem.1069>.
- [8] Yan Wang and Hai-Ping Cheng. “Oxygen Reduction Activity on Perovskite Oxide Surfaces: A Comparative First-Principles Study of LaMnO<sub>3</sub>, LaFeO<sub>3</sub>, and LaCrO<sub>3</sub>”. In: *The Journal of Physical Chemistry C* 117.5 (2013), pp. 2106–2112. DOI: 10.1021/jp309203k. eprint: <https://doi.org/10.1021/jp309203k>. URL: <https://doi.org/10.1021/jp309203k>.
- [9] J. K. Nørskov et al. “Origin of the Overpotential for Oxygen Reduction at a Fuel-Cell Cathode”. In: *The Journal of Physical Chemistry B* 108.46 (2004), pp. 17886–17892. DOI: 10.1021/jp047349j. eprint: <https://doi.org/10.1021/jp047349j>. URL: <https://doi.org/10.1021/jp047349j>.
- [10] Zhiyao Duan and Guofeng Wang. “Comparison of Reaction Energetics for Oxygen Reduction Reactions on Pt(100), Pt(111), Pt/Ni(100), and Pt/Ni(111) Surfaces: A First-Principles Study”. In: *The Journal of Physical Chemistry C* 117.12 (2013), pp. 6284–6292. DOI: 10.1021/jp400388v. eprint: <https://doi.org/10.1021/jp400388v>. URL: <https://doi.org/10.1021/jp400388v>.
- [11] Michael F. Peintinger, Daniel Vilela Oliveira, and Thomas Bredow. “Consistent Gaussian basis sets of triple-zeta valence with polarization quality for solid-state calculations”. In: *Journal of Computational Chemistry* 34.6 (2013), pp. 451–459. DOI: <https://doi.org/10.1002/jcc.23153>. eprint: <https://onlinelibrary.wiley.com/doi/pdf/10.1002/jcc.23153>. URL: <https://onlinelibrary.wiley.com/doi/abs/10.1002/jcc.23153>.
- [12] R. Korotana et al. “Hybrid density functional study of structural, bonding, and electronic properties of the manganite series La<sub>1-x</sub>Ca<sub>x</sub>MnO<sub>3</sub> ( $x = 0, \frac{1}{4}, 1$ )”. In: *Phys. Rev. B* 89 (20 May 2014), p. 205110. DOI: 10.1103/PhysRevB.89.205110. URL: <https://link.aps.org/doi/10.1103/PhysRevB.89.205110>.
- [13] Chengteh Lee, Weitao Yang, and Robert G. Parr. “Development of the Colle-Salvetti correlation-energy formula into a functional of the electron density”. In: *Phys. Rev. B* 37 (2 Jan. 1988), pp. 785–789. DOI: 10.1103/PhysRevB.37.785. URL: <https://link.aps.org/doi/10.1103/PhysRevB.37.785>.
- [14] S. H. Vosko, L. Wilk, and M. Nusair. “Accurate spin-dependent electron liquid correlation energies for local spin density calculations: a critical analysis”. In: *Canadian Journal of Physics* 58.8 (1980), pp. 1200–1211. DOI: 10.1139/p80-159. eprint: <https://doi.org/10.1139/p80-159>. URL: <https://doi.org/10.1139/p80-159>.

- [15] P. J. Stephens et al. “Ab Initio Calculation of Vibrational Absorption and Circular Dichroism Spectra Using Density Functional Force Fields”. In: *The Journal of Physical Chemistry* 98.45 (1994), pp. 11623–11627. DOI: 10.1021/j100096a001. eprint: <https://doi.org/10.1021/j100096a001>. URL: <https://doi.org/10.1021/j100096a001>.
- [16] Roberto Dovesi et al. “Quantum-mechanical condensed matter simulations with CRYSTAL”. In: *WIREs Computational Molecular Science* 8.4 (2018), e1360. DOI: <https://doi.org/10.1002/wcms.1360>. eprint: <https://onlinelibrary.wiley.com/doi/pdf/10.1002/wcms.1360>. URL: <https://onlinelibrary.wiley.com/doi/abs/10.1002/wcms.1360>.
- [17] Nilima Sinha and Srimanta Pakhira. “Tunability of the Electronic Properties of Covalent Organic Frameworks”. In: *ACS Applied Electronic Materials* 3.2 (2021), pp. 720–732. DOI: 10.1021/acsaem.0c00867. eprint: <https://doi.org/10.1021/acsaem.0c00867>. URL: <https://doi.org/10.1021/acsaem.0c00867>.
- [18] Jon Baker, Andrew Scheiner, and Jan Andzelm. “Spin contamination in density functional theory”. In: *Chemical Physics Letters* 216.3 (Dec. 1993), pp. 380–388. DOI: 10.1016/0009-2614(93)90113-F.
- [19] Alejandro Montoya, Thanh N. Truong, and Adel F. Sarofim. “Spin Contamination in Hartree–Fock and Density Functional Theory Wavefunctions in Modeling of Adsorption on Graphite”. In: *The Journal of Physical Chemistry A* 104.26 (2000), pp. 6108–6110. DOI: 10.1021/jp000534m. eprint: <https://doi.org/10.1021/jp000534m>. URL: <https://doi.org/10.1021/jp000534m>.
- [20] Hendrik J. Monkhorst and James D. Pack. “Special points for Brillouin-zone integrations”. In: *Phys. Rev. B* 13 (12 June 1976), pp. 5188–5192. DOI: 10.1103/PhysRevB.13.5188. URL: <https://link.aps.org/doi/10.1103/PhysRevB.13.5188>.
- [21] Koichi Momma and Fujio Izumi. “VESTA 3 for three-dimensional visualization of crystal, volumetric and morphology data”. In: *Journal of Applied Crystallography* 44.6 (2011), pp. 1272–1276. DOI: <https://doi.org/10.1107/S0021889811038970>. eprint: <https://onlinelibrary.wiley.com/doi/pdf/10.1107/S0021889811038970>. URL: <https://onlinelibrary.wiley.com/doi/abs/10.1107/S0021889811038970>.
- [22] Mois I. Aroyo et al. “Brillouin-zone database on the *Bilbao Crystallographic Server*”. In: *Acta Crystallographica Section A* 70.2 (Mar. 2014), pp. 126–137. DOI: 10.1107/S205327331303091X. URL: <https://doi.org/10.1107/S205327331303091X>.

- [23] Tasci, E.S. et al. “An introduction to the tools hosted in the Bilbao Crystallographic Server”. In: *EPJ Web of Conferences* 22 (2012), p. 00009. DOI: 10.1051/epjconf/20122200009. URL: <https://doi.org/10.1051/epjconf/20122200009>.
- [24] Priyadarshini Parida et al. “Universality in the electronic structure of 3d transition metal oxides”. In: *Journal of Physics and Chemistry of Solids* 123 (2018), pp. 133–149. ISSN: 0022-3697. DOI: <https://doi.org/10.1016/j.jpcs.2018.04.009>. URL: <https://www.sciencedirect.com/science/article/pii/S002236971830204X>.
- [25] Wojciech Paszkowicz et al. “Lattice parameters and orthorhombic distortion of CaMnO<sub>3</sub>”. In: *Powder Diffraction* 25.1 (2010), pp. 46–59. DOI: 10.1154/1.3314256.
- [26] Jun Xu et al. “Recent Advances in Oxygen Electrocatalysts Based on Perovskite Oxides”. eng. In: *Nanomaterials (Basel, Switzerland)* 9.8 (Aug. 2019). nano9081161[PII], p. 1161. ISSN: 2079-4991. DOI: 10.3390/nano9081161. URL: <https://doi.org/10.3390/nano9081161>.
- [27] Yueh-Lin Lee et al. “Ab initio energetics of LaBO<sub>3</sub>(001) (*B* = Mn, Fe, Co, and Ni) for solid oxide fuel cell cathodes”. In: *Phys. Rev. B* 80 (22 Dec. 2009), p. 224101. DOI: 10.1103/PhysRevB.80.224101. URL: <https://link.aps.org/doi/10.1103/PhysRevB.80.224101>.
- [28] Min Ho Seo et al. “Design of Highly Active Perovskite Oxides for Oxygen Evolution Reaction by Combining Experimental and ab Initio Studies”. In: *ACS Catalysis* 5.7 (2015), pp. 4337–4344. DOI: 10.1021/acscatal.5b00114. eprint: <https://doi.org/10.1021/acscatal.5b00114>. URL: <https://doi.org/10.1021/acscatal.5b00114>.
- [29] Srimanta Pakhira, Kevin P. Lucht, and Jose L. Mendoza-Cortes. “Iron Intercalation in Covalent–Organic Frameworks: A Promising Approach for Semiconductors”. In: *The Journal of Physical Chemistry C* 121.39 (2017), pp. 21160–21170. DOI: 10.1021/acs.jpcc.7b06617. eprint: <https://doi.org/10.1021/acs.jpcc.7b06617>. URL: <https://doi.org/10.1021/acs.jpcc.7b06617>.
- [30] Srimanta Pakhira and Jose L. Mendoza-Cortes. “Quantum Nature in the Interaction of Molecular Hydrogen with Porous Materials: Implications for Practical Hydrogen Storage”. In: *The Journal of Physical Chemistry C* 124.11 (2020), pp. 6454–6460. DOI: 10.1021/acs.jpcc.9b11939. eprint: <https://doi.org/10.1021/acs.jpcc.9b11939>. URL: <https://doi.org/10.1021/acs.jpcc.9b11939>.

- [31] Srimanta Pakhira and Jose L. Mendoza-Cortes. “Tuning the Dirac Cone of Bilayer and Bulk Structure Graphene by Intercalating First Row Transition Metals Using First-Principles Calculations”. In: *The Journal of Physical Chemistry C* 122.9 (2018), pp. 4768–4782. DOI: 10.1021/acs.jpcc.7b11761. eprint: <https://doi.org/10.1021/acs.jpcc.7b11761>. URL: <https://doi.org/10.1021/acs.jpcc.7b11761>.
- [32] Mats Johnsson and Peter Lemmens. “Crystallography and Chemistry of Perovskites”. In: *Handbook of Magnetism and Advanced Magnetic Materials*. American Cancer Society, 2007. ISBN: 9780470022184. DOI: <https://doi.org/10.1002/9780470022184.hmm411>. eprint: <https://onlinelibrary.wiley.com/doi/pdf/10.1002/9780470022184.hmm411>. URL: <https://onlinelibrary.wiley.com/doi/abs/10.1002/9780470022184.hmm411>.
- [33] Weber Duarte Mesquita et al. “Barium strontium titanate-based perovskite materials from DFT perspective: assessing the structural, electronic, vibrational, dielectric and energetic properties”. In: *Theoretical Chemistry Accounts* 140.3 (Feb. 2021), p. 27. ISSN: 1432-2234. DOI: 10.1007/s00214-021-02723-2. URL: <https://doi.org/10.1007/s00214-021-02723-2>.
- [34] Yuan Cheng et al. “Enhancing Oxygen Exchange Activity by Tailoring Perovskite Surfaces”. In: *The Journal of Physical Chemistry Letters* 10.14 (2019). PMID: 31271532, pp. 4082–4088. DOI: 10.1021/acs.jpclett.9b01235. eprint: <https://doi.org/10.1021/acs.jpclett.9b01235>. URL: <https://doi.org/10.1021/acs.jpclett.9b01235>.
- [35] Yu-Qi Lyu and Francesco Ciucci. “Activating the Bifunctionality of a Perovskite Oxide toward Oxygen Reduction and Oxygen Evolution Reactions”. In: *ACS Applied Materials & Interfaces* 9.41 (2017). PMID: 28948763, pp. 35829–35836. DOI: 10.1021/acsami.7b10216. eprint: <https://doi.org/10.1021/acsami.7b10216>. URL: <https://doi.org/10.1021/acsami.7b10216>.
- [36] Joaquín Soriano-López, Wolfgang Schmitt, and Max García-Melchor. “Computational modelling of water oxidation catalysts”. In: *Current Opinion in Electrochemistry* 7 (2018), pp. 22–30. ISSN: 2451-9103. DOI: <https://doi.org/10.1016/j.coelec.2017.10.001>. URL: <https://www.sciencedirect.com/science/article/pii/S2451910317301242>.
- [37] Ryan Jacobs et al. “Assessing Correlations of Perovskite Catalytic Performance with Electronic Structure Descriptors”. In: *Chemistry of Materials* 31.3 (2019), pp. 785–797. DOI: 10.1021/acs.chemmater.8b03840. eprint: <https://doi.org/10.1021/acs.chemmater.8b03840>. URL: <https://doi.org/10.1021/acs.chemmater.8b03840>.